J. Synchrotron Rad. (1999). **6**, 34–42

EXAFS analysis of the L_3 edge of Ce in CeO_2: effects of multi-electron excitations and final-state mixed valence

E. Fonda,[a] D. Andreatta,[a] P. E. Colavita[a] and G. Vlaic[a,b]*

[a]*Dipartimento di Scienze Chimiche, Università degli Studi di Trieste, Via L. Giorgieri 1, 34127 Trieste, Italy, and* [b]*Sincrotrone Trieste SCpA, SS 14, Km 163.5, 34012 Trieste, Italy. E-mail: vlaic@elettra.trieste.it*

(*Received 15 May 1998; accepted 28 July 1998*)

Cerium oxide (IV) (CeO_2) is extensively employed in heterogeneous catalysis, particularly as a promoter of noble metal action in three-way catalysts. For this reason there is a great scientific and economical interest in the development of any possible chemical or structural analysis technique that could provide information on these systems. EXAFS spectroscopy has revealed itself as a powerful technique for structural characterization of such catalysts. Unfortunately, good quality *K*-edge spectra of cerium are not yet easily obtainable because of the high photon energy required (>40 keV). On the other hand, at lower energies it is easy to collect very good spectra of the L_3 edge (5.5 keV), but L_3-edge spectra of cerium (IV) are characterized by the presence of two undesired additional phenomena that interfere with EXAFS analysis: final-state mixed-valence behaviour and intense multi-electron excitations. Here, a comparative analysis of the *K*, L_3, L_2 and L_1 edges of Ce in CeO_2 has been made and a procedure for obtaining structural parameters from L_3-edge EXAFS, even in the presence of these features, has been developed. This procedure could allow further studies of catalytic compounds containing tetravalent cerium surrounded by oxygen ligands.

Keywords: EXAFS; CeO_2; multielectron excitations; final-state mixed valence.

1. Introduction

Cerium oxide (IV) (CeO_2) is extensively employed in heterogeneous catalysis, particularly as a promoter of noble metal action in three-way catalysts (Fornasiero *et al.*, 1995; Ranga Rao *et al.*, 1995).

EXAFS spectroscopy has revealed itself as a powerful technique for structural characterization of such catalytic systems (Vlaic *et al.*, 1997; Li *et al.*, 1994*a*,*b*). At present, by using synchrotron light devices, it is possible to record high-quality EXAFS spectra for a large variety of elements for a detailed quantitative analysis. However, for heavy elements like cerium, good quality *K*-edge spectra are not yet easily obtainable because of the high photon energy required (>40 keV). On the other hand, at lower energies it is possible to collect very good spectra of the L_3 edge (5.5 keV). However, the L_3-edge spectrum of cerium (IV) is characterized by the presence of two undesired additional phenomena: final-state mixed-valence behaviour and intense multi-electron excitations. These phenomena interfere with EXAFS analysis. The goal of our work is to obtain a correct L_3-edge EXAFS analysis procedure for obtaining structural parameters even in the presence of these features. This procedure could allow further studies of catalytic compounds containing tetravalent cerium surrounded by oxygen ligands.

In many Ce compounds, strong resonant-like features are superimposed on the EXAFS signal at about 120 eV over the edge. These features are due to multi-electron excitations and are evident in disordered materials (Solera *et al.*, 1995; Chaboy *et al.*, 1990, 1994). Moreover, tetravalent Ce compounds show a peculiar double-peak shape of the L_3 edge (Fig. 1). This is due to the mixed-valence behaviour of tetravalent Ce in its final state, due to the interaction between 4*f* orbitals of the metal and 2*p* orbitals of the ligands in its initial state (Bianconi *et al.*, 1987; Soldatov *et al.*, 1994; Malterre, 1990; Natoli & Benfatto, 1987; Beaurepoire *et al.*, 1988). This is a final-state effect which tends to lower the EXAFS signal amplitude (Solera *et al.*, 1995).

For obtaining a quantitative evaluation of the effect of the different phenomena on structural parameters, we made a comparative analysis of *K*, L_3, L_2 and L_1 edges of Ce in CeO_2. First of all we simulated the *K*-edge EXAFS signal and we found that it was quite simple to obtain a fairly good agreement with experimental data; the structural parameters obtained were compatible with crystallographic data. From this starting point we began to analyse the L_3-edge EXAFS signal. Using the same procedure we expected to obtain a result similar to that obtained for *K*-edge EXAFS signal analysis, but we found big discrepancies between L_3- and *K*-edge EXAFS signal analysis

Table 1
Structure of the first five atomic shells around Ce in CeO_2.

Shell number	Atom	N	Distance (Å)
1	O	8	2.343
2	Ce	12	3.828
3	O	24	4.487
4	Ce	6	5.411
5	O	24	5.896

results. By careful comparison of the two data sets we identified two distinct phenomena interfering with the L_3-edge EXAFS signal analysis.

We clearly identified two strong multi-electron excitations on the L_3 and L_2 edges. We found that it is necessary to use two sets of theoretical phases and amplitudes in order to correctly fit the EXAFS amplitude of the L_3 edge. This method has been used by other authors for performing an L_3-edge XANES simulation of Ce in CeO_2 (Soldatov *et al.*, 1994).

2. Experimental details

Analysis was carried out on two spectra, whose recording conditions were the following:

(i) K edge of Ce in CeO_2 (room temperature): the absorption spectrum was collected on the GILDA beamline (BM8) at the ESRF storage ring. The monochromator was an Si(511) double crystal. The first ionization chamber was filled with Kr at a pressure of 0.235 atm, the second was filled with Kr at 1 atm. The sample was prepared by grinding carefully 100 mg of CeO_2 (Aldrich 99.99%) together with 100 mg of polyethylene in a mortar. The homogeneity of the sample was checked by moving it in the two directions perpendicular to the X-ray beam, keeping the energy of the X-rays constant and controlling whether the absorption coefficient of the sample remained constant or not.

(ii) L_3, L_2 and L_1 edges of Ce in CeO_2 (room temperature): the absorption spectrum was collected on EXAFS-II, station E4, at the DORIS storage ring. The monochromator was an Si(111) double crystal. Harmonics were rejected detuning the crystal while using stabilization feedback control. The sample was prepared by deposition from a powder suspension in cyclohexane on a Millipore membrane (type RA 12 μm).

3. Analysis details

The space group of CeO_2 is $Fm3m$ with cell parameter a = 5.411 Å (Wyckoff, 1963). The independent positions in this cell are Ce at 0,0,0 and O at 0.25,0.25,0.25. In the structure we can identify successive coordination shells around the Ce atom. Data referring to the first five shells are reported in Table 1.

Data analysis was performed using the *GNXAS* package (Filipponi & Cicco, 1995). *GNXAS* was used because it is the only currently available software which introduces special parameters into the simulation to describe multi-electron excitation features. *GNXAS* also produces reliable relativistic treatment of the EXAFS signal, suitable for heavy atoms like Ce.

Due to the high quality of the data of all spectra we k^2-weighted all EXAFS signals during parameter refining and in all the figures.

The value of S_0^2 (amplitude reduction factor) in all cases was taken as fixed and equal to unity in all simulations in spite of the fact that usually its fitted value should range from 0.8 to 0.95 (Filipponi *et al.*, 1995). When S_0^2 was left free to vary it did not change its value significantly from unity.

The values of the energy resolution parameter are described in the tables and in the following paragraphs.

3.1. *Analysis of the K-edge EXAFS*

We fitted data in k-space in the interval 2.9–10.4 $Å^{-1}$ (equivalent to an energy interval 40482–40863 eV). Actually, the quality of the spectrum allowed the upper limit to be extended to 15 $Å^{-1}$, but in order to make a comparison between K- and L_3-edge spectra we chose a shorter interval. In fact, the presence of the L_2 edge in the L_3-edge spectrum prevents a fit beyond 10.4 $Å^{-1}$ from being performed. The approximate experimental resolution of the GILDA beamline at 40 keV is 4 eV. We allowed the value of the energy resolution to be free to vary in the fitting and we found a final value of the energy resolution of 5.6 eV; this is in agreement with a further broadening due to the finite core-hole lifetime.

We tested how many scattering paths were necessary to obtain a good simulation of the EXAFS signal and to

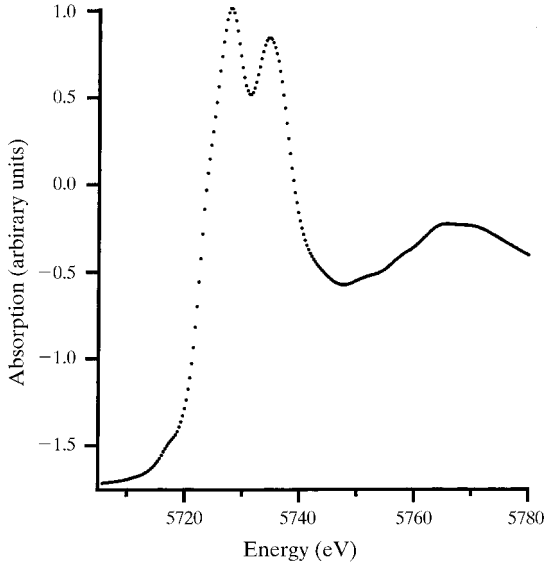

Figure 1
L_3 edge of Ce in CeO_2. The double-peak shape of the edge is mainly due to two transitions: the lower-energy peak is assigned to the $2p \rightarrow 5d$ transition with $4f^1\underline{L}$ configuration, the higher-energy peak to the $2p \rightarrow 5d$ transition with $4f^0L$ configuration.

obtain the best agreement between structural parameters calculated by EXAFS signal fitting and crystallographic data.

First we introduced the single-scattering contributions due to the first four shells of atomic neighbours into the simulation. The comparison between the EXAFS simulated signals including the contribution of shells (1), (2), (3) and (4) and the experimental EXAFS signal are displayed in Fig. 2(*a*), and Fig. 2(*b*) reports the single-scattering contribution of each shell to the simulation with four shells. The agreement between experimental and simulated EXAFS signals was fairly good and the FFT of the simulated signal matched the FFT of the experimental EXAFS signal from 0 to 4 Å (Fig. 3). The introduction of more single-scattering contributions into the calculations did not really improve the quality of the simulation or the obtained data; in fact, even the fourth-shell contribution is small, though not negligible.

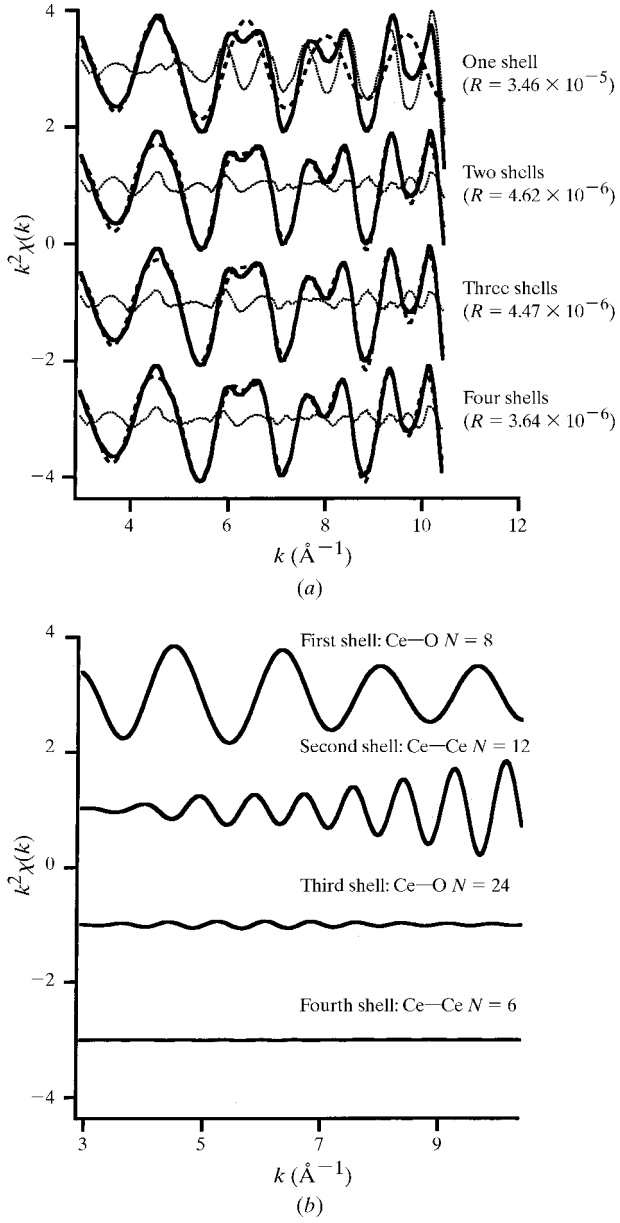

Figure 2
(*a*) Different number of shells in the EXAFS simulation. Continuous line: experimental signal; dashed line: simulation; dots: residual. (*b*) Single-scattering contributions added to the simulation.

Then we introduced the effect of multiple scattering into the simulation. We considered in our calculations only the most important scattering paths, *i.e.* geometrical arrangements of three atoms with deviations from collinearity below 60°, paths with the number of scattering processes below six and with a maximum length of 8 Å. The results of these calculations are reported in Table 2.

The improvement of the simulation obtained by adding the multiple scattering was negligible compared with the number of free parameters added. Moreover, the values of the structural parameters obtained from the calculations with and without the multiple-scattering effects are in good agreement. For these reasons we decided to use only the single-scattering approximation to simulate all the EXAFS signals presented in this work.

3.2. *L_3-edge EXAFS analysis*

We used the same four-shell model [model (1) in Figs. 4(*a*) and 4(*b*)] for L_3-edge analysis, but the EXAFS simulation was not in good agreement with the experimental signal (see Table 3).

Then we introduced a shake-up resonance into the simulation [model (3) in Figs. 4(*a*) and 4(*b*)]. In fact, evidence of the presence of multi-electron excitations in the Ce L_3-edge EXAFS energy region has been shown by several authors (Solera *et al.*, 1995; Chaboy *et al.*, 1990, 1994; Kodre *et al.*, 1995). To simulate this feature we used a Lorentzian curve characterized by three parameters

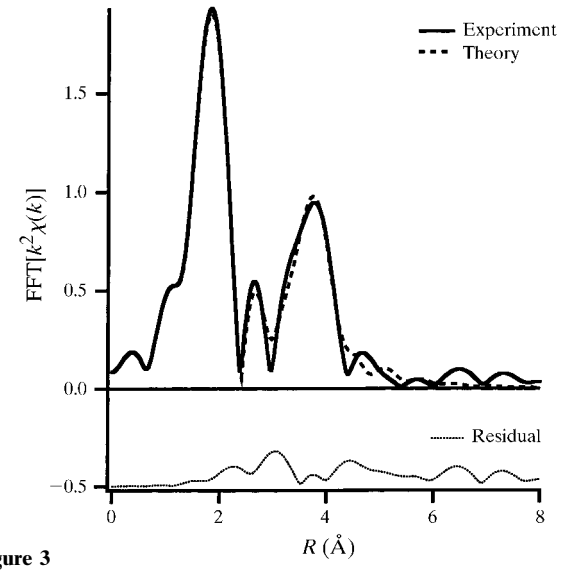

Figure 3
FFT of experimental *K*-edge EXAFS (continuous line), four-shell simulation (dashed line) and residual (dots). The residual is vertically down-shifted for clarity.

Table 2
Comparison of single- and multiple-scattering approximations of *K*-edge EXAFS.

Models	Four-shell single scattering	Multiple scattering (angles fixed)	Multiple scattering (angles varying)
Ce—O			
N	8	8	8
R (Å)	2.35 ± 0.02	2.345	2.353
σ^2 (10^{-3} Å^2)	2.8 ± 1.6	2.9	2.2
Ce—Ce			
N	12	12	12
R (Å)	3.863 ± 0.012	3.857	3.868
σ^2 (10^{-3} Å^2)	4.0 ± 0.6	4.1	3.9
Ce—O			
N	24	24	24
R (Å)	4.53 ± 0.03	4.54	4.52
σ^2 (10^{-3} Å^2)	13 ± 4	12	14
Ce—Ce			
N	6	6	6
R (Å)	5.42 ± 0.02	5.41	5.43
σ^2 (10^{-3} Å^2)	7 ± 4	10	5.6
O—Ce—O			
Angle (deg)		180	171
σ^2 (deg^2)		35	0.43
Ce—Ce—Ce			
Angle (deg)		120	127
σ^2 (deg^2)		0.93	0.0
Ce—Ce—Ce			
Angle (deg)		180	182
σ^2 (deg^2)		36	43
E_0 (eV)	40455 ± 3	40454	40455
S_0^2	1.0	1.0	1.0
Experimental resolution (eV)	5.6 ± 0.2	5.7	5.7
Residual	3.64×10^{-6}	3.55×10^{-6}	3.01×10^{-6}

(position, height and width) which could freely vary during the fit procedure (Fig. 5*a*). This additional feature improved the fit, which matched better the experimental signal. Although the residual was smaller than that of model (1), its value and the values of the structural parameters were still far from those obtained from the *K*-edge spectrum (see Table 3). It was necessary to introduce another correction.

To take into account the mixed-valence behaviour of Ce^{IV} we approximated the L_3-edge EXAFS signal with two EXAFS signals which differed only in their *k*-scale origin and in the relative weight of the signal amplitude [model (4) in Table 3]. To perform this with *GNXAS* we introduced two sets of phases and amplitudes with different *k*-scale origins (two phases and amplitudes for each simulated shell), *i.e.* we simply changed the energy scale of one calculated set. The energy difference between the origins was 7 eV and we assigned a 66% relative weight to the phase and amplitude with the origin at lowest energy.

The energy difference between the two origins and the weights of the functions were kept constant in the fit, so we did not introduce any additional parameter in this step of the simulation. Once again the residual decreased compared with model (1). This last model, labelled (4) in Figs. 4(*a*) and 4(*b*), matched the L_3-edge EXAFS as good as the simplest model matched the *K*-edge EXAFS.

We also tried one more model. We introduced the double set of phases and amplitudes without the correction for the multi-electron excitation. This model was labelled (2) and

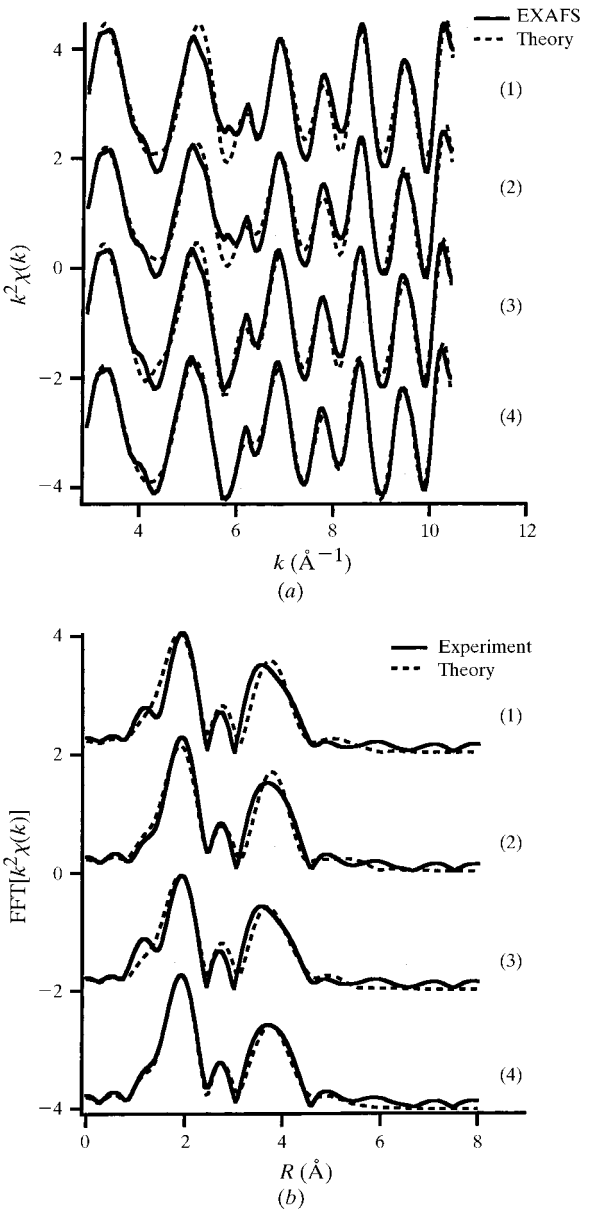

Figure 4
(*a*) L_3-edge EXAFS simulation with different models. (*b*) FFT of experimental and theoretical EXAFS. Residuals are not reported for clarity (see Table 2). Model (1): four single-scattering shells were used to simulate experimental EXAFS. Model (2): the previous model was modified and two theoretical EXAFS signals shifted by 7 eV were used; the amplitude ratio of the lower-energy signal to the higher-energy signal is 3:2. Model (3): the multi-electron excitation has been subtracted from the experimental EXAFS, but two theoretical EXAFS signals were not used in the simulation. Model (4): the multi-electron excitation was subtracted from the experimental EXAFS and two theoretical EXAFS signals were used in the simulation, as described in model (2).

Table 3
Comparison of structural data and residuals obtained with different models, edges and techniques.

	L_3-edge					Crystallographic
	Model (1)	Model (2)	Model (3)	Model (4)	K-edge	data
Ce—O						
N	8	8	8	8	8	8
R (Å)	2.306 ± 0.001	2.319 ± 0.003	2.320 ± 0.003	2.336 ± 0.003	2.35 ± 0.02	2.343
σ^2 (10^{-3} Å^2)	7.0 ± 0.1	6.4 ± 0.3	6.0 ± 0.6	4.40 ± 0.5	2.8 ± 1.6	
Ce—Ce						
N	12	12	12	12	12	12
R (Å)	3.856 ± 0.002	3.859 ± 0.002	3.857 ± 0.002	3.862 ± 0.003	3.863 ± 0.012	3.826
σ^2 (10^{-3} Å^2)	4.7 ± 0.2	3.7 ± 0.2	4.7 ± 0.2	3.7 ± 0.2	4.0 ± 0.6	
Ce—O						
N	24	24	24	24	24	24
R (Å)	4.483 ± 0.004	4.42 ± 0.01	4.51 ± 0.01	4.46 ± 0.01	4.53 ± 0.03	4.487
σ^2 (10^{-3} Å^2)	20 ± 1	17 ± 1	20 ± 1	15 ± 1	13 ± 4	
Ce—Ce						
N	6	6	6	6	6	6
R (Å)	5.40 ± 0.01	5.40 ± 0.03	5.41 ± 0.01	5.40 ± 0.01	5.42 ± 0.02	5.411
σ^2 (10^{-3} Å^2)	5 ± 2	6 ± 3	5 ± 1	5 ± 1	7 ± 4	
E_0 (eV)	5731.0 ± 0.2	5729.7 ± 0.2	5731.4 ± 0.2	5730.3 ± 0.2	40455 ± 3	
S_0^2	1.0	1.0	1.0	1.0	1.0	
Experimental resolution (eV)	4.0	4.0	4.0	4.0	5.6 ± 0.2	
Multi-electron excitations						
Position (eV)	–	–	5854.2 ± 0.8	5854.3 ± 0.6	–	
Height percentage of edge jump	–	–	2.8% ± 0.5	3.4% ± 0.1	–	
Width (eV)	–	–	9 ± 3	9.6 ± 1.2	–	
Residual	1.02×10^{-4}	6.53×10^{-5}	7.41×10^{-5}	3.04×10^{-5}	3.64×10^{-6}	

again, without introducing any additional free parameter, the residual was significantly lower than that of model (1) [Table 3 and Figs. 4(*a*) and 4(*b*)].

It is important to carefully introduce broadening due to finite core-hole lifetime and experimental resolution into the EXAFS simulation. For the L_3 edge we used a sum of 1 eV for the estimated experimental resolution (EXAFS-II beamline at DORIS storage ring) and 3 eV for the core-hole lifetime as reported in the literature (Soldatov *et al.*, 1994). However, if we vary the resolution parameter in the L_3 fitting without using two-channels convolution, we find an abnormal broadening of 8 eV or even more. This is due to an evident error in the model amplitude.

3.3. *L_2-edge EXAFS analysis*

We also tried to extend our analysis to the L_2- and L_1-edge EXAFS signals to confirm the data obtained from L_3-edge EXAFS analysis, moreover to verify if it was possible to use jointly these edges for obtaining more accurate structural data.

Data for the L_2 and L_1 edges reported in all of the tables and figures have always been obtained from simultaneous multi-edge fitting. No independent fit of the L_2 and L_1 edges is reported herein, because their EXAFS signals are superimposed on EXAFS signals of the preceding edge, *i.e.* the L_2-edge EXAFS signal is superimposed on the L_3-edge EXAFS signal which does not stop at the energy where the L_2-edge appears. Thus we always used the same structural parameters fitting L_3, L_2 and L_1 edges together as when we fitted the L_3-edge EXAFS signal alone. Then we subtracted the extrapolated simulation of the EXAFS signals of lower-energy edges from the highest one. With this method we were able to fit two or more EXAFS signals with the same structural parameters and greatly increase the number of independent points. This is a standard feature of the *GNXAS* package (Di Cicco, 1996).

We fitted the L_2-edge EXAFS signal between 2.9 and 9.8 Å^{-1} in k-space.

Using the multi-edge fitting procedure, only the not simulated (or in other words 'residual') signal of the L_3 edge cannot be subtracted from the L_2-edge EXAFS signal. This residual signal of the L_3-edge was not negligible; in this way the simulation of the L_2-edge EXAFS signal was not as good as that of the L_3-edge EXAFS signal (Fig. 6).

Incidentally, the simulation was good enough to provide further information. In fact, on the L_2 edge it was necessary to introduce a resonance, like on the L_3 edge. Its position, relative to E_0 and its width were similar to those on the L_3 edge and the intensity ratio between the resonances was approximately equal to the intensity ratio between the edge jumps (Fig. 5*b*).

It is difficult to say in this case if it is necessary or not to use two different sets of phases and amplitudes. The lowering of the residual due to the addition of the shifted set of phases and amplitudes is not as significant as that found on the L_3 edge, even trying different constant values for the energy gap between the origins of the k scale and the relative intensity of the two channels.

Table 4
L_3, L_2 and L_1 multiple edge fit results.

Parameters			
Ce−O			
N	8		
R (Å)	2.334 ± 0.003		
σ^2 (10^{-3} Å^2)	4.7 ± 0.3		
Ce−Ce			
N	12		
R (Å)	3.859 ± 0.003		
σ^2 (10^{-3} Å^2)	4.0 ± 0.1		
Ce−O			
N	24		
R (Å)	4.457 ± 0.006		
σ^2 (10^{-3} Å^2)	17 ± 1		
Ce−Ce			
N	6		
R (Å)	5.407 ± 0.008		
σ^2 (10^{-3} Å^2)	5 ± 1		
	L_3	L_2	L_1
E_0 (eV)	5730.2 ± 0.2	6171.1 ± 0.2	6553.3 ± 0.4
S_0^2	1.0	1.0	1.0
Experimental resolution (eV)	4.0	4.0	4.0
Multi-electron excitations	L_3	L_2	
Position (eV)	5854.4 ± 0.6	6294.6 ± 0.8	
Height percentage of edge jump	3.4% ± 0.1	4% ± 1	
Width (eV)	10.7 ± 0.6	11 ± 1	
Residual	1.02×10^{-4}		

This is probably due to the complexity and difficulty of the L_2-edge EXAFS fit. In fact, the residual of the fit at low k-scale values is significantly greater than that found on the L_3 edge, probably for the non-completely subtracted L_3-edge EXAFS signal superimposed on the L_2-edge. In this way the effect of the two energy-shifted sets, which is greater at low k values, seems to be less important than on the L_3 edge.

For these reasons we do not report herein the results on the use of two sets of phases and amplitudes on the L_2 edge; the data obtained without the two sets are reported in Table 4.

3.4. *L_1-edge EXAFS analysis*

We analysed the L_1-edge EXAFS signal in the interval 3.5–9.8 Å^{-1} in the same way as we analysed that of the L_2 edge. We fitted simultaneously L_3-, L_2- and L_1-edge EXAFS signals (Table 4). The simulation was not good in terms of superimposing the L_3- and L_2-edge EXAFS signals. The same observation has been performed on the L_2-edge EXAFS signal simulation. In this case it was unnecessary to introduce two sets of phases and amplitudes and additional background shake-up features (Fig. 6*c*). In fact we found no evidence for a relevant shake-up feature, though it was found in less complex Ce^{IV} systems and described by other authors (Solera *et al.*, 1995; Chaboy *et al.*, 1994).

3.5. *Error bars calculation*

We calculated the error bars of the parameters by the Monte Carlo method (Kalos & Whitlock, 1986). We estimated the average noise level of each spectrum using different smoothing procedures and we found values of about 10^{-3}. Then we produced a sample population of spectra adding a random noise with normal distribution and a standard deviation equal to 10^{-3}. On each element of the sample population we applied the same fitting procedure using the *SIMPLEX* routine (*MINUIT*, 1992). During

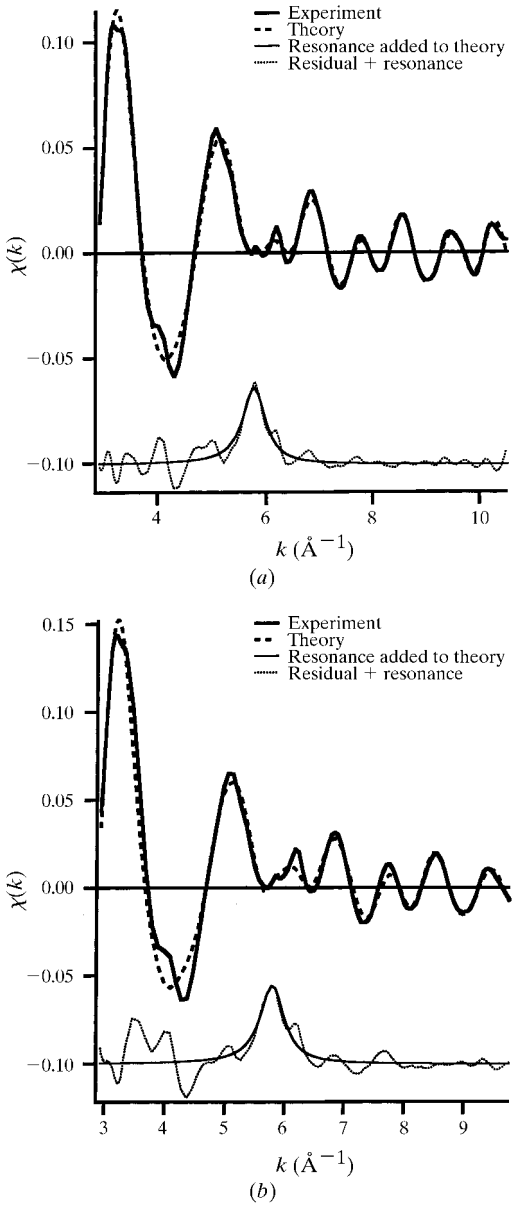

Figure 5
(*a*) Simulation of the L_3-edge EXAFS with model (4) (see text and Fig. 4 for description). (*b*) Simulation of the L_2-edge EXAFS (see text for model used). Large continuous lines: experimental EXAFS signals; dashed lines: sum of the theoretical EXAFS and multi-electron excitation; narrow continuous line: simulated multi-electron excitation; dots: sum of the residual and multi-electron excitation.

the fitting we allowed the background removal parameters to be free, in order to include into the error bars the correlation between background and structural parameters. We performed many tests on the number of elements of the sample population to be used and we found that the error bars became fairly constant using more than 15 spectra, so we built a population of 20 elements.

Estimated standard deviations (e.s.d.s) and averaged values were obtained by averaging the different fit results and assuming a normal distribution. We also calculated correlation coefficients with standard formulae (Taylor, 1990). We always used a sample population of 20 elements and this lead to a confidence interval for the e.s.d. of each parameter of, at most, 20% of its value (Spiegel, 1979). Tables reported on this paper show errors calculated with a 95.28% confidence level (*i.e.* a confidence interval as large as twice the e.s.d.).

To routinely perform such calculations with *GNXAS* we developed a set of codes. In this way we can apply a more robust method for error analysis than gradient-based routines.

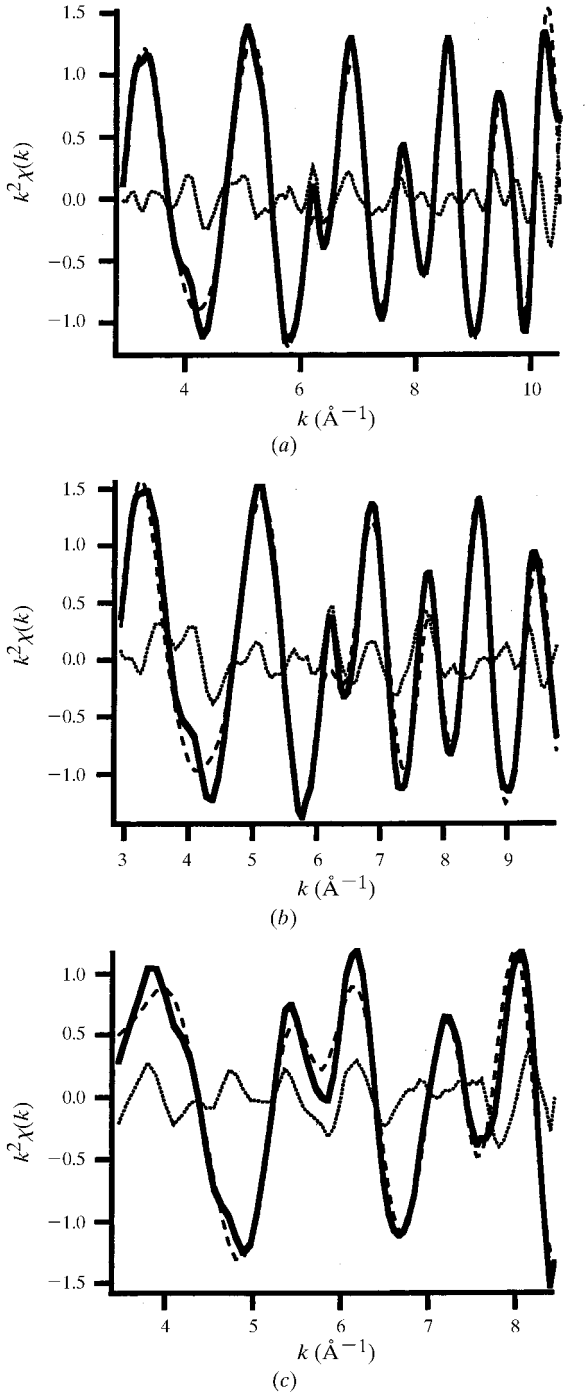

Figure 6
Multi-edge refining of (*a*) L_3-edge, (*b*) L_2-edge and (*c*) L_1-edge EXAFS; the same structural parameters are used to fit simultaneously the three signals. Continuous line: experimental EXAFS signal; dashed line: theoretical EXAFS; dots: residual. In (*a*) and (*b*) the multi-electron excitation has been subtracted from the experimental EXAFS.

4. Discussion

It is evident, from the examined data, that a simple EXAFS simulation is unable to provide good results and that it is necessary to introduce simultaneously the effect of mixed-valence behaviour and multi-electron excitation.

The introduction of two different sets of phases and amplitudes lowers considerably the residual with no cost in terms of the number of variable parameters. This implies a damping of the EXAFS spectrum, especially at low k-scale values, which is in agreement with the differences found by other authors (Solera *et al.*, 1995) when comparing the L_3-edge EXAFS signals of similar compounds of Ce^{III} and Ce^{IV}.

The use of the two shifted EXAFS signals [*i.e.* model (4)] is based on the possibility of calculating independently the electron excitation process for the two different electronic configurations ($4f^0L$ and $4f^1\underline{L}$, if we neglect $4f^2\underline{L}$). Such an approximation is the same as that used for XANES simulations performed by other authors (Bianconi *et al.*, 1987; Soldatov *et al.*, 1994; Malterre, 1990). In fact, these two electronic configurations lead to a different screening of the core hole: the peak at a lower energy can be interpreted as a $2p \rightarrow 5d$ transition with a $4f^1\underline{L}$ initial-state configuration, whereas that at a higher energy can be interpreted as a $2p \rightarrow 5d$ transition with a $4f^0L$ initial state.

Our results confirm the necessity of using such an approach when simulating an EXAFS signal.

The correction of the multi-electron excitations has been performed carefully. It is particularly evident, comparing models (2) and (4) in Figs. 4(*a*) and 4(*b*), that the discrepancies between data and simulation are essentially localized in a narrow region. Moreover, the evident shoulder on the left of the first FFT peak disappears after having introduced the correction for the multi-electron excitation. This is due to the removal of the non-periodic feature. In addition, after removal of the multi-electron excitation, the first-shell distance increased, becoming closer to the crystallographic estimate.

These multi-electron excitations, assigned to $2p$, $4d \rightarrow 5d^2$ transitions (Chaboy *et al.*, 1994), have a similar relative position on the L_3 and L_2 edges (124 eV and 123 eV above the edge, respectively) and their intensity ratio is near to 2:1, equal to their edge-jump ratio. These experimental values are in agreement with the degeneracy ratio of the L_3 and L_2 final states: $j = 3/2$ and $j = 1/2$.

One more observation can be performed on the values of the disorder parameters of the first shells. Introducing the corrections to the model their values lower significantly, approaching values calculated independently on the *K*-edge spectrum. Furthermore, we want to point out that it is important to carefully introduce broadening due to finite core-hole lifetime and experimental resolution into the EXAFS simulation.

Although it is evident that the simulation of the L_3-edge spectrum improves using model (4), simulation of the L_2 spectrum does not improve significantly using the same model. In principle, both the L_3- and L_2-edge EXAFS simulations should improve as we introduce the correction, but the overlap of the L_3-edge EXAFS signal onto that of the L_2 edge makes the analysis more difficult. In fact, the effect of mixing two EXAFS signals with different edge positions is stronger at lower k (Å^{-1}) values and negligible at higher ones, but on the L_2 edge at low k values the mixing of the L_2-EXAFS and L_3-EXAFS residual is also strong. In this way it is not easy to find a clear difference between the models and we do not report these data here.

5. Conclusions

Several theoretical and experimental papers have been written on multi-electron excitations in Ce^{III} and Ce^{IV} compounds (Solera *et al.*, 1995; Chaboy *et al.*, 1990, 1994; Kodre *et al.*, 1995; Mukoyama & Ito, 1994), but in all cases it was possible to identify the phenomenon in the XAS spectra only in poorly structured materials with simple or weak EXAFS signals.

We identified two multi-electron excitations, present in both L_3 and L_2 edges of a highly structured material like a metal oxide (CeO_2) where the EXAFS signal is strong and complex. This allowed a more accurate determination of distances and further analysis of the EXAFS structure.

We found that the simultaneous use of two distinct energy-shifted signals is necessary for the correct simulation of the L_3-edge EXAFS, as suggested in previous XANES studies (Bianconi *et al.*, 1987; Soldatov *et al.*, 1994) and experimental observations (Solera *et al.*, 1995).

The L_3 edge of CeO_2 is a particularly complex quantistic puzzle, though the common use in the EXAFS community of experimental phases and amplitudes and analysis performed through Fourier filtering of the first shell have hidden the real problems and the complexity of this system. In fact, both phenomena were generally known but, only now, using accurate theoretical calculations and studying the entire unfiltered EXAFS signal, have we felt it necessary to put all of the pieces together. The recent development of advanced analysis software has played a major role in making affordable and routinely available *ab-initio* EXAFS simulations, but in this way it is not possible to neglect additional quantistic phenomena like multi-electron excitations or mixed-valence behaviours.

This work now allows us to use the same technique on the analysis of the L_3 edge of Ce in $Ce_xZr_{1-x}O_2$ catalysts. These are important real catalytic systems and they will be the subject of further studies. In the spectra of high-surface-area catalysts the greater structural disorder will diminish the amplitude of the EXAFS signal revealing more clearly the multi-electron excitations features. For the same reason the overlap of the L_3- and L_2-EXAFS signal on the L_2 edge will be smaller allowing a better L_2-edge simulation. This means that multi-electron excitation removal and the use of a double EXAFS channel will be of critical importance for the correct evaluation of distances and coordination numbers.

We thank the Sincrotrone Trieste ScpA for economical support and computer assistance. We fully acknowledge the authors of *GNXAS* and *FITHEO* software for user license and support. We thank Dr Obaidur Rahman for the recording of the L_3-, L_2- and L_1-edge data set at the EXAFS-II beamline of DORIS storage ring in Hamburg. We thank Dr Paolo Ghigna for sample preparation and recording of the *K*-edge data set at ESRF on the GILDA beamline.

References

Beaurepoire, E., Kappler, J., Malterre, D. & Krill, O. (1988). *Europhys. Lett.* **5**, 369–374.
Bianconi, A., Marcelli, A., Dexpert, H., Karnatak, R., Kotani, A., Jo, T. & Petiau, J. (1987). *Phys. Rev. B*, **35**, 806–812.
Chaboy, J., Garcìa, J., Marcelli, A. & Ruiz-López, M. F. (1990). *Chem. Phys. Lett.* **174**, 389–395.
Chaboy, J., Marcelli, A. & Tyson, T. A. (1994). *Phys. Rev. B*, **49**, 11652–11661.
Di Cicco, A. (1996). *Phys. Rev. B*, **53**, 6174–6185.
Filipponi, A. & Di Cicco, A. (1995). *Phys. Rev. B*, **52**, 15135–15149.
Filipponi, A., Di Cicco, A. & Natoli, C. R. (1995). *Phys. Rev. B*, **52**, 15122–15134.
Fornasiero, P., Di Monte, R., Ranga Rao, G., Kaspar, J., Meriani, S., Trovarelli, A. & Graziani, M. (1995). *J. Catal.* **151**, 168–177.
Kalos, M. H. & Whitlock, P. A. (1986). *Monte Carlo Methods.* New York: John Wiley and Sons.
Kodre, A., Arcon, I., Hribar, M., Stuhec, M., Villain, F., Drube, W. & Tröger, L. (1995). *Physica B*, **208/209**, 379–380.
Li, P., Chen, I.-W. & Penner-Hahn, J. E. E. (1994*a*). *J. Am. Ceram. Soc.* **77**, 118–128.
Li, P., Chen, I.-W. & Penner-Hahn, J. E. E. (1994*b*). *J. Am. Ceram. Soc.* **77**, 1281–1288.
Malterre, D. (1990). *Phys. Rev. B*, **43**, 1391–1398.
MINUIT (1992). *Reference Manual*. Version 92.1, CERN Program Library Long Writeup D506. CERN, Geneva, Switzerland.
Mukoyama, T. & Ito, Y. (1994). *Nucl. Instrum. Methods Phys. Res. B*, **87**, 26–33.
Natoli, C. R. & Benfatto, M. (1987). *Springer Ser. Solid State Sci.* **81**, 184–190.

Ranga Rao, G., Fornasiero, P., Kaspar, J., Meriani, S., Di Monte, R. & Graziani, M. (1995). *Stud. Surf. Sci. Catal.* **96**, 631–643.

Soldatov, A. V., Ivanchenko, T. S., Della Longa, S., Kotani, A., Iwamoto, Y. & Bianconi, A. (1994). *Phys. Rev. B*, **50**, 5074–5080.

Solera, J. A., García, J. & Proietti, M. G. (1995). *Phys. Rev. B*, **51**, 2678–2686.

Spiegel, M. R. (1979). *Collana SCHAUM, Probabilità e Statistica*, pp. 197–198. Milano: ETAS Libri.

Taylor, J. K. (1990). *Statistical Techniques for Data Analysis*, pp. 137–139. Boca Raton: CRC Press.

Vlaic, G., Fornasiero, P., Geremia, S., Kaspar, J. & Graziani, M. (1997). *J. Catal.* **168**, 386–392.

Wyckoff, R. W. G. (1963). *Crystal Structure.* New York: Interscience.